

Article

# Chemical Vapor Transport Deposition of Molybdenum Disulfide Layers Using H<sub>2</sub>O Vapor as the Transport Agent

Shichao Zhao \*, Jiaxin Weng, Shengzhong Jin, Yanfei Lv and Zhenguo Ji \*

College of Materials & Environmental Engineering, Hangzhou Dianzi University, Hangzhou 310018, China; weng\_jiaxin@126.com (J.W.); wk\_jsz@163.com (S.J.); lvyfanfei@hdu.edu.cn (Y.L.)

\* Correspondence: zhaoshichao@hdu.edu.cn (S.Z.); jizg@hdu.edu.cn (Z.J.)

Received: 8 January 2018; Accepted: 14 February 2018; Published: 21 February 2018

**Abstract:** Molybdenum disulfide (MoS<sub>2</sub>) layers show excellent optical and electrical properties and have many potential applications. However, the growth of high-quality MoS<sub>2</sub> layers is a major bottleneck in the development of MoS<sub>2</sub>-based devices. In this paper, we report a chemical vapor transport deposition method to investigate the growth behavior of monolayer/multi-layer MoS<sub>2</sub> using water (H<sub>2</sub>O) as the transport agent. It was shown that the introduction of H<sub>2</sub>O vapor promoted the growth of MoS<sub>2</sub> by increasing the nucleation density and continuous monolayer growth. Moreover, the growth mechanism is discussed.

**Keywords:** chemical vapor transport deposition; molybdenum disulfide; monolayer; water; mechanism

## 1. Introduction

Molybdenum disulfide (MoS<sub>2</sub>) layers, having unique optical and electrical properties, have attracted extensive interest in the fields of energy generation, electronics, and sensors [1–7]. The growth of large-scale, high-quality MoS<sub>2</sub> layers targeted for silicon integrated device fabrication is still challenging. Vapor deposition has been the predominant method for the growth of large-scale, continuous MoS<sub>2</sub> monolayer or few layers films in recent years [8–10]. Molybdenum oxides and sulfur are generally used as precursors of MoS<sub>2</sub>. For example, Lee et al. heated MoO<sub>3</sub> powder in sulfur vapor and obtained MoS<sub>2</sub> monolayer and multi-layer films [11]. In this method, MoO<sub>3</sub> was first reduced by sulfur vapor to form MoO<sub>3-x</sub>, which was then further reacted with sulfur vapor to form MoS<sub>2</sub> [12]. MoO<sub>3</sub> acted as a nucleation center promoting crystal growth as well as the introduction of crystal defects. The introduction of defects plays two important roles; one is to promote nucleation for multi-layer growth, and the other is to tailor the electrical properties [13–16]. The MoS<sub>2</sub> domains grown with this method showed different morphologies, e.g. triangle, hexagon, three-point star, as a function of the different atomic ratio of sulfur to molybdenum [17,18].

MoS<sub>2</sub> powder is another commonly used starting material. Wu et al. [19] heated MoS<sub>2</sub> powder at 900 °C in the center of a tube furnace and obtained a MoS<sub>2</sub> monolayer on an insulating substrate downstream of the precursor in a lower temperature zone (~650 °C). The usage of single-precursor MoS<sub>2</sub> powder as the source of Mo and S avoided the introduction of impurities and heterogeneous nucleation during the growth of MoS<sub>2</sub> flakes. Therefore, the MoS<sub>2</sub> monolayer showed a regular triangular shape and high optical quality. This vapor-solid growth method is suitable for the deposition of high-quality monolayer single crystal flake. However, in our recent work, we found that the nucleation is difficult to initiate and the growth temperature window is very narrow, ca. ~50 °C [20]. These issues could be attributed to the low vapor pressure of MoS<sub>2</sub> powder. The chemical vapor transport method was generally used for the growth of crystals with a solid precursor that has low vapor pressure. For example, Pisoni et al. reported the growth of MoS<sub>2</sub> single crystals using I<sub>2</sub>, Br<sub>2</sub>, and TeCl<sub>4</sub> as transport agents [21]. The transport agent converts MoS<sub>2</sub> into high vapor pressure

intermediates, which undergo the reverse reaction to deposit MoS<sub>2</sub> onto the substrate. However, the vapor transport agents used in this study are highly toxic and reactive, which could limit their widespread use.

To overcome this limitation, we have investigated ways to improve the nucleation density of MoS<sub>2</sub> using various additives. In this paper, we report the chemical vapor transport growth behavior of MoS<sub>2</sub> monolayer or multi-layer films by using MoS<sub>2</sub> powder as the precursor and water (H<sub>2</sub>O) vapor as the transport agent. In the nucleation stage, H<sub>2</sub>O vapor was introduced into the deposition system and acted as a chemical transport agent. Our mechanistic study suggests that water reacted with MoS<sub>2</sub> to form MoO<sub>2</sub>, which promoted the nucleation of MoS<sub>2</sub>. In the previously mentioned growth methods, the sulfur comes from the sublimation of sulfur or MoS<sub>2</sub> powder and the sulfur flow rate is out of control. Here, the sulfur was formed through the reaction of MoS<sub>2</sub> and water, which provides us a possible way to adjust the sulfur flow rate by controlling the water vapor flow rate. In the second stage, H<sub>2</sub>O vapor was cut off and MoS<sub>2</sub> continuously grew through a simple physical vapor transport process. This novel approach combined the heterogeneous nucleation and homogeneous growth to control the crystal size and thickness of the MoS<sub>2</sub> layer. The thickness of the MoS<sub>2</sub> film obtained ranged from a monolayer to multiple layers. The lateral size of the single-crystal domain is up to 300 μm.

## 2. Materials and Methods

### MoS<sub>2</sub> Layers Synthesis

MoS<sub>2</sub> was prepared by modifying a previously reported vapor deposition method using a silicon wafer with a 300-nm layer of oxide (SiO<sub>2</sub>/Si) as the substrate [19]. The schematic of the vapor deposition setup is shown in Figure 1. MoS<sub>2</sub> powder (99.5% purity, Aladdin, Shanghai, China) was used as the precursor. Before use, the precursor (0.5 g) was loaded into a small quartz glass boat (70 mm in length) and put in the center of the tube furnace (1 inch in diameter, Hefei Kejing Materials technology Co. Ltd., Hefei, China). Before growth, the precursor was flushed under Ar/H<sub>2</sub> (70 sccm, H<sub>2</sub> 5%, total pressure of 75 Torr. sccm: standard cubic centimeter per minute) for 10 min at room temperature to remove the air and water absorbed on the precursor. The substrate was put downstream close to the furnace wall.

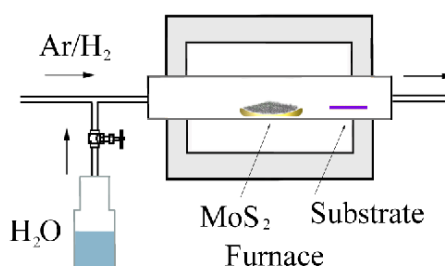


Figure 1. Schematic illustration of the MoS<sub>2</sub> growth setup.

For the MoS<sub>2</sub> growth, the precursor was heated to 1000 °C from room temperature in 30 min under Ar/H<sub>2</sub> (75 Torr, Ar/H<sub>2</sub> 70 sccm) and kept at 1000 °C for 1 h. The furnace was then turned off and cooled from 1000 °C to room temperature. During the above heating process, the temperature of the substrate ranged from 710 to 850 °C. The water (H<sub>2</sub>O) vapor was introduced into the furnace by turning on/off the water valve, which connects the water tube and the Ar/H<sub>2</sub> inlet. For typical growth, the water valve was kept open during the whole heating stage. For studies on the influence of H<sub>2</sub>O on the growth of MoS<sub>2</sub>, we kept the valve open during the heating stage but limited the water exposure during the synthesis.

Optical microscope imaging of the sample was conducted with a Jiangnan MV3000 digital microscope (Nanjing Jiangnan Novel Optics Co. Ltd., Nanjing, China). Tapping mode atomic force microscopy (AFM) was performed on an Agilent 5500 (Agilent Technologies, Palo Alto, CA, USA) in air. Raman spectrum and photoluminescence (PL) were acquired on a Renishaw Via micro-Raman spectroscope (Renishaw, London, UK) with a 532 nm solid-state laser at room temperature. X-ray diffraction (XRD) was carried on a Thermo ARLXTRA (Thermo Electron, Waltham, USA) and ultraviolet visible diffuse reflection spectroscopy (UV-Vis DRS, not including specular reflection) was performed on Shimadzu MPC-3100 (Shimadzu, Tokyo, Japan) with an integrating sphere.

### 3. Results and Discussion

#### 3.1. MoS<sub>2</sub> Flakes Grown in the Presence of H<sub>2</sub>O Vapor

MoS<sub>2</sub> flakes were prepared on the substrate using H<sub>2</sub>O and MoS<sub>2</sub> powder as illustrated in Figure 2a. Figure 2b shows the separated triangular MoS<sub>2</sub> flakes grown on the SiO<sub>2</sub>/Si substrate with the H<sub>2</sub>O vapor valve kept open during the heating of the furnace and growth of the MoS<sub>2</sub> flakes. The thickness of the flakes ranged from monolayer to multiple layers. The triangles in dim and uniform color indicate the uniform monolayer MoS<sub>2</sub>. The bright color triangles are attributed to multi-layer MoS<sub>2</sub> with a pyramid-shape structure. The flake lateral size ranged from ca. 20 to 40 μm.

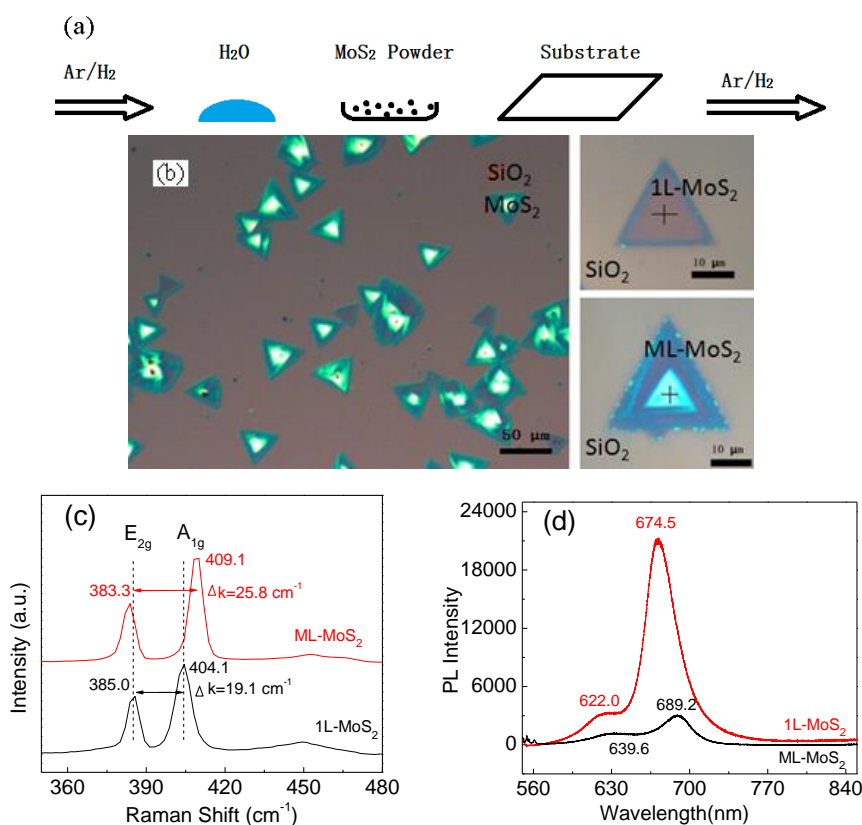


**Figure 2.** (a) Schematic illustration of the MoS<sub>2</sub> growth using H<sub>2</sub>O and MoS<sub>2</sub> powder; (b) Optical images of MoS<sub>2</sub> grown on a SiO<sub>2</sub>/Si substrate with H<sub>2</sub>O vapor for 10 min; (c) Typical Raman spectra and (d) Photoluminescence (PL) spectra of the monolayer (1L-MoS<sub>2</sub>) and multi-layer MoS<sub>2</sub> (ML-MoS<sub>2</sub>) flakes according images shown in Figure 2b.

The success of the growth and thickness of the MoS<sub>2</sub> flakes were confirmed by Raman spectroscopy. Figure 2c displays the typical Raman spectra of monolayer and multi-layer MoS<sub>2</sub> flakes corresponded to the images in Figure 2b. The E<sub>2g</sub> and A<sub>1g</sub> modes of MoS<sub>2</sub> were observed. The frequency difference

between the  $E_{2g}$  and  $A_{1g}$  mode is thickness-dependent. With the increase of the layer number, the frequency difference will increase. The  $E_{2g}$  and  $A_{1g}$  peaks positions are at  $385.0\text{ cm}^{-1}$  and  $404.1\text{ cm}^{-1}$  ( $383.3\text{ cm}^{-1}$  and  $409.1\text{ cm}^{-1}$ ) with a frequency difference of  $19.9\text{ cm}^{-1}$  ( $25.8\text{ cm}^{-1}$ ), indicating that the thickness of flakes is monolayer (multi-layer) [22].

Besides Raman spectra, PL is generally used for the identification of the thickness of the  $\text{MoS}_2$ . Mak et al. studied the relationship between the PL quantum yield and layer number. They found that the PL quantum yield drops quickly with the increase of the layer number. Bulk  $\text{MoS}_2$  is an indirect-gap semiconductor showing negligible PL. Few-layer  $\text{MoS}_2$  shows weak PL due to the confinement effects. Monolayer  $\text{MoS}_2$  is a direct-gap semiconductor giving out bright PL [23]. Figure 2d shows the typical photoluminescence spectra (PL) both of the monolayer and multi-layer  $\text{MoS}_2$  flakes corresponded to the images in Figure 2b. The excitation wavelength was 532 nm. The PL peaks of monolayer  $\text{MoS}_2$  are located at 674.5 nm and 622 nm, which are attributed to the A1 and B1 direct excitonic transition emission of the  $\text{MoS}_2$  monolayer, respectively [9,17,24]. We observed that the PL intensity of the monolayer is much stronger than that of the multi-layer sample.

### 3.2. Effect of $\text{H}_2\text{O}$ Vapor on the $\text{MoS}_2$ Layers Growth

To investigate the effect of  $\text{H}_2\text{O}$  vapor on the  $\text{MoS}_2$  growth, we limited the time the synthesis was exposed to water vapor. After the precursors were heated to  $1000\text{ }^\circ\text{C}$ , the water valve was closed after a fixed amount of time during the growth stage: Figure 3a–d 0 min (least water exposure), Figure 3e–h 10 min, Figure 3i–l 20 min, and Figure 3m–p 60 min (most water exposure).

Shown in Figure 3a–d, the shape of the  $\text{MoS}_2$  prepared without the introduction of  $\text{H}_2\text{O}$  is a separated island. Meanwhile in Figure 3e,i–k,m–o, continuous, large-area  $\text{MoS}_2$  films were observed. This may be due to the presence of  $\text{H}_2\text{O}$  vapor, which enhanced the diffusibility of molybdenum and sulfur atoms at domain boundaries, resulting in the continuous growth of monolayer  $\text{MoS}_2$ . The large optical contrast in Figure 3e–p indicates the formation of multiple layers and/or clusters, which may be due to the formation of high heterogeneous nucleation density and the Stranski-Krastanov growth mode. The formation of heterogeneous nucleation will be discussed below. Besides the continuous film obtained as described above, the domain size of  $\text{MoS}_2$  prepared with  $\text{H}_2\text{O}$  (shown in Figure 3f–h,p) was larger than those prepared without  $\text{H}_2\text{O}$  (shown in Figure 3b,c). Figure 4 shows the magnified optical image of the same sample that is shown in Figure 3e. The lateral size of the triangle-shaped  $\text{MoS}_2$  flakes ranges from  $24\text{ }\mu\text{m}$  to  $372\text{ }\mu\text{m}$ . The average lateral size of the  $\text{MoS}_2$  flakes prepared without  $\text{H}_2\text{O}$  introduction was  $13 \pm 6\text{ }\mu\text{m}$ , while the average size increased to  $159 \pm 80\text{ }\mu\text{m}$  based on the statistical calculation of the size of the isolated flakes shown in Figure 3a–h, respectively.

The water introduction also has an effect on the thickness of  $\text{MoS}_2$  flakes. Based on the frequency difference ( $24.7\text{ cm}^{-1}$ , Figure S1) between the  $E_{2g}$  and  $A_{1g}$  mode of  $\text{MoS}_2$  and uniform color contrast, we can conclude that the  $\text{MoS}_2$  flakes prepared without water exposure in Figure 3a–d is multi-layer. In contrast, in those samples prepared in the presence of water (Figure 3e–p), monolayer  $\text{MoS}_2$  was observed (as discussed at the end of Section 3.2). Therefore, the introduction of water can reduce the thickness of the  $\text{MoS}_2$  flakes.

It is reported that water molecules and carbon atoms can intercalate between the two-dimensional material and the substrate [25–27]. Although we do not have enough evidence to show the presence of the water intercalation in our sample at high growth temperature ( $710\text{ }^\circ\text{C}$  to  $850\text{ }^\circ\text{C}$ ), we suspect that the molecular structure of water vapor possibly intercalates into the interlayer of the  $\text{MoS}_2$  flakes or the interface between the  $\text{MoS}_2$  and  $\text{SiO}_2/\text{Si}$  substrate, which affects the absorption, desorption, and diffusion of the precursor atoms and even the final monolayer growth.

From Figure 3m–o, we can observe some bright features. The white spots are multi-layer  $\text{MoS}_2$ . The area with green and yellow color we suspected to be amorphous  $\text{MoS}_2$ ,  $\text{MoO}_2$ , or even organic contamination. To reduce the organic contamination, the silicon wafer substrate was cleaned with hot piranha solution (7:3 concentrated  $\text{H}_2\text{SO}_4$ :35%  $\text{H}_2\text{O}_2$ ) for 10 min at room temperature, and the vapor deposition system was flushed under  $\text{Ar}/\text{H}_2$  to remove air-borne contamination before  $\text{MoS}_2$  growth.

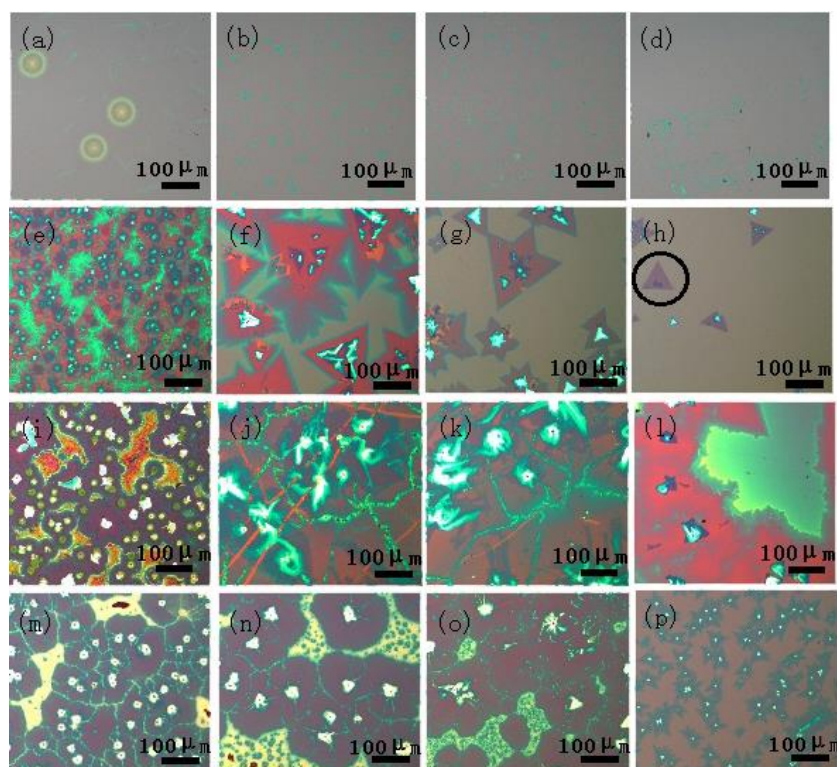


**Figure 3.** Optical images of the MoS<sub>2</sub> grown on a SiO<sub>2</sub>/Si substrate with varying the amount of H<sub>2</sub>O vapor released into the furnace. The images in each row are of the same sample but measured at different areas. From the left to right, the deposition temperature decreases as a result of the differences in the location. The amount of H<sub>2</sub>O vapor into the furnace is controlled by adjusting the length of time that the H<sub>2</sub>O valve is open: (a–d) 0 min; (e–h) 10 min; (i–l) 20 min; and (m–p) 60 min. For (f,j,k), we intentionally scratched the sample to show the contrast between the MoS<sub>2</sub> film and the SiO<sub>2</sub>/Si substrate (bright orange color). The scale bars represent 100 μm.

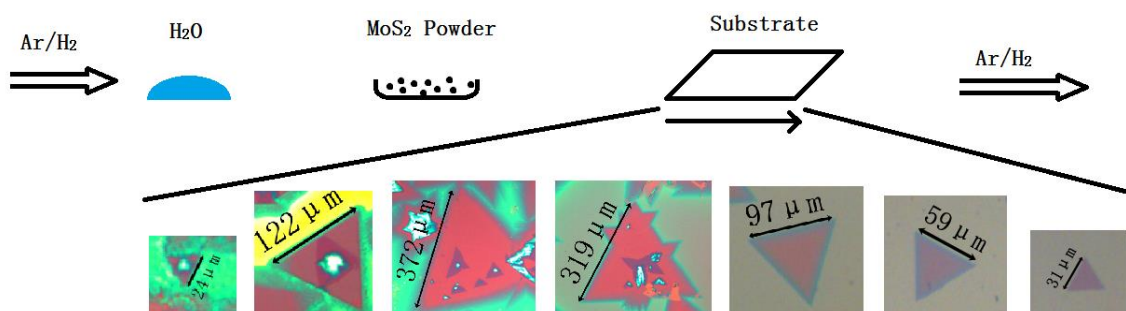


**Figure 4.** Magnified optical images of the same sample that is shown in Figure 3e. The images were measured at different locations. From left to right, the growth temperature was gradually decreasing.

Figure 5 shows the typical UV-Vis DRS of the MoS<sub>2</sub> film corresponding to the images shown in Figure 3e–h. The UV-Vis DRS peaks at 665 and 610 nm match the two PL emission peaks (Figure 2d), and are due to the characteristic A1 and B1 direct excitonic transitions of MoS<sub>2</sub>, respectively [28].

AFM is a commonly used technique for two-dimensional material thickness measurement. Here, we conducted multiple scans of the thickness of the monolayer MoS<sub>2</sub> at an edge of the MoS<sub>2</sub> flake by AFM. Figure 6 shows the typical AFM image of the edge of the monolayer MoS<sub>2</sub> triangle shown circled in black in Figure 3h. A straight trench with a width of ca. 150 nm was observed on the

substrate surface, which divided the substrate into two sections. The bottom of the trench is the  $\text{SiO}_2/\text{Si}$  substrate. The left side of the trench is  $\text{MoS}_2$  particles, and the right side of the trench is monolayer  $\text{MoS}_2$ . The thickness of the  $\text{MoS}_2$  flake is  $0.9 \pm 0.1\text{nm}$  (Figure 6, Figure S2, and Table S1), indicating that the flake is monolayer. This thickness value, although it significantly deviates from the expected thickness of monolayer  $\text{MoS}_2$  (0.615 nm), is consistent with other AFM measurements of single-layer  $\text{MoS}_2$  deposited on a  $\text{SiO}_2$  substrate [29,30]. In fact, the discrepancy that the measured value by AFM is larger than the theoretical value is common phenomena in the measurement of the thickness of two-dimensional monolayer materials, such as graphene [31]. The discrepancy was attributed to the instrument offset due to tip-substrate interaction as well as adsorbed molecules between the monolayer and the  $\text{SiO}_2$  substrate [26,31]. From the AFM image in Figure 6, we can see that monolayer  $\text{MoS}_2$  is smooth and continuous. We measured the root-mean-square (RMS) surface roughness over a  $1\ \mu\text{m} \times 1\ \mu\text{m}$  area. The RMS was 0.22 nm. The trench is probably formed through the rapid diffusion of  $\text{MoS}_2$  nucleation along the direction perpendicular to the domain edge. Detailed study of the trench will be reported in future study. In addition to the trench, there are also many white particles on the surface of the  $\text{MoS}_2$  flake. These particles should be  $\text{MoS}_2$  formed during the growth of the  $\text{MoS}_2$  flake, or even contaminations formed during the transport of the sample.

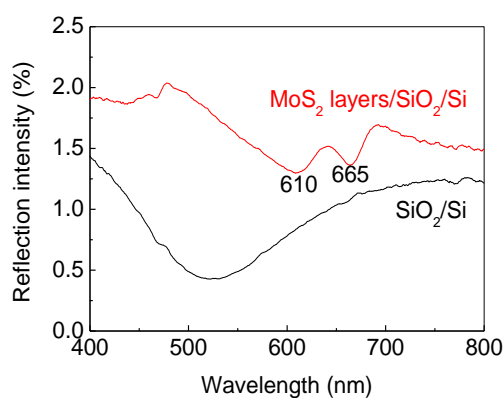


**Figure 5.** Typical ultraviolet visible diffuse reflection spectroscopy (UV-Vis DRS) of  $\text{MoS}_2$  corresponding to the images in Figure 3b.

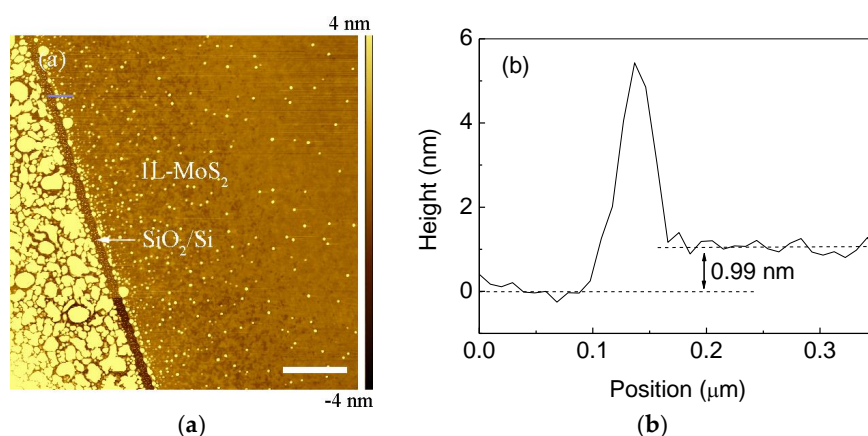


**Figure 6.** Atomic force microscopy (AFM) image (a) and cross-section (b) (along the blue line marked in (a)) of monolayer  $\text{MoS}_2$  grown on the  $\text{SiO}_2/\text{Si}$  substrate corresponding to the images in Figure 3h. The scale bars represent  $1\ \mu\text{m}$  in AFM image.

### 3.3. Mechanism of MoS<sub>2</sub> Growth in the Presence of H<sub>2</sub>O Vapor

The results obtained in Figure 3 suggest that H<sub>2</sub>O vapor promoted the growth of MoS<sub>2</sub> film. We hypothesized that the H<sub>2</sub>O vapor reacted with MoS<sub>2</sub> powder to give molybdenum oxide. Then the molybdenum oxide evaporated and deposited on the substrate, acting as heterogeneous nucleation center, from which the molybdenum oxide reacted with sulfur at a lower temperature and transformed into the MoS<sub>2</sub> layer [12]. The following reactions should have occurred during the growth of MoS<sub>2</sub> [32]:



To verify this hypothesis experimentally, we used XRD to test the composition of the precursor annealed at 1000 °C for 20 h in H<sub>2</sub>O vapor and H<sub>2</sub>/Ar atmosphere. We indeed found that all of the XRD peaks in Figure 7 were indexed according to the monoclinic molybdenum dioxide (MoO<sub>2</sub>) (JCPDS NO. 00-032-0671). This result agrees with our hypothesis that molybdenum oxide was formed. The growth process essentially is a chemical vapor transport process. The H<sub>2</sub>O vapor acts as transport agent.

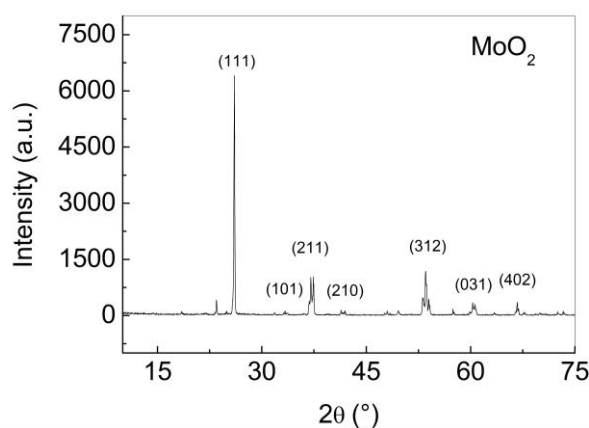


**Figure 7.** X-ray diffraction (XRD) of MoS<sub>2</sub> powder after annealing in Ar/H<sub>2</sub> and H<sub>2</sub>O vapor at 1000 °C for 12 h. The peak positions are indexed to monoclinic MoO<sub>2</sub> (JCPDS NO. 00-032-0671).

## 4. Conclusions

In summary, we have successfully prepared monolayer/multi-layer MoS<sub>2</sub> through a H<sub>2</sub>O vapor-modified vapor deposition method on a SiO<sub>2</sub>/Si substrate. The growth of MoS<sub>2</sub> is highly sensitive to the presence of H<sub>2</sub>O. The results reveal that H<sub>2</sub>O increases the nucleation density of MoS<sub>2</sub> flakes. The Raman, PL, and AFM revealed that both monolayer and multi-layer MoS<sub>2</sub> were formed. Under extended water exposure, a continuous MoS<sub>2</sub> film was formed. Using XRD, we showed that MoO<sub>2</sub> was formed by the reaction between MoS<sub>2</sub> and water, which resulted in the observed enhancement in the nucleation and growth.

**Supplementary Materials:** The following are available online at <http://www.mdpi.com/2079-6412/8/2/78/s1>, Figure S1: Raman spectra of a multi-layers MoS<sub>2</sub> growth on the SiO<sub>2</sub>/Si substrate tested at different locations, corresponding to the data in Figure 3a–d; Figure S2: AFM image of monolayer MoS<sub>2</sub> showing the edge of the domain. Scale bar represents 1 μm in AFM image; Table S1: Average height of the monolayer MoS<sub>2</sub> corresponding to the data in Figure S2 and Figure 6.

**Acknowledgments:** This work was supported by the Natural Science Foundation of Zhejiang Province, China Projects (LY16E020008) and Chinese NSF Projects (61106100). We thank Haitao Liu (Department of Chemistry, University of Pittsburgh, USA) for his kind assistance with data analysis and paper writing.

**Author Contributions:** Shichao Zhao conceived and designed the experiments and wrote the paper; Jiaxin Weng, Shengzhong Jin and Yanfei Lv performed the experiments; Shichao Zhao and Zhenguo Ji analyzed the data.

**Conflicts of Interest:** The authors declare no conflict of interest.

## References

1. Buscema, M.; Barkelid, M.; Zwiller, V.; van der Zant, H.S.J.; Steele, G.A.; Castellanos-Gomez, A. Large and tunable photothermoelectric effect in single-layer MoS<sub>2</sub>. *Nano Lett.* **2013**, *13*, 358–363. [[CrossRef](#)] [[PubMed](#)]
2. Li, X.X.; Fan, Z.Q.; Liu, P.Z.; Chen, M.L.; Liu, X.; Jia, C.K.; Sun, D.M.; Jiang, X.W.; Han, Z.; Bouchiat, V.; et al. Gate-controlled reversible rectifying behaviour in tunnel contacted atomically-thin MoS<sub>2</sub> transistor. *Nat. Commun.* **2017**, *8*, 970. [[CrossRef](#)] [[PubMed](#)]
3. Naylor, C.H.; Kybert, N.J.; Schneier, C.; Xi, J.; Romero, G.; Saven, J.G.; Liu, R.Y.; Johnson, A.T.C. Scalable production of molybdenum disulfide based biosensors. *ACS Nano* **2016**, *10*, 6173–6179. [[CrossRef](#)] [[PubMed](#)]
4. Shavanova, K.; Bakakina, Y.; Burkova, I.; Shteplyuk, I.; Viter, R.; Ubelis, A.; Beni, V.; Starodub, N.; Yakimova, R.; Khranovskyy, V. Application of 2D non-graphene materials and 2D oxide nanostructures for biosensing technology. *Sensors* **2016**, *16*, 223. [[CrossRef](#)] [[PubMed](#)]
5. Kalantar-zadeh, K.; Ou, J.Z. Biosensors based on two-dimensional MoS<sub>2</sub>. *ACS Sens.* **2016**, *1*, 5–16. [[CrossRef](#)]
6. Lopez-Sanchez, O.; Lembke, D.; Kayci, M.; Radenovic, A.; Kis, A. Ultrasensitive photodetectors based on monolayer MoS<sub>2</sub>. *Nat. Nanotechnol.* **2013**, *8*, 497–501. [[CrossRef](#)] [[PubMed](#)]
7. Tsai, M.L.; Su, S.H.; Chang, J.K.; Tsai, D.S.; Chen, C.H.; Wu, C.I.; Li, L.J.; Chen, L.J.; He, J.H. Monolayer MoS<sub>2</sub> heterojunction solar cells. *ACS Nano* **2014**, *8*, 8317–8322. [[CrossRef](#)] [[PubMed](#)]
8. Robertson, J.; Liu, X.; Yue, C.L.; Escarra, M.; Wei, J. Wafer-scale synthesis of monolayer and few-layer MoS<sub>2</sub> via thermal vapor sulfurization. *2D Mater.* **2017**, *4*, 045007. [[CrossRef](#)]
9. Kim, Y.; Bark, H.; Ryu, G.H.; Lee, Z.; Lee, C. Wafer-scale monolayer MoS<sub>2</sub> grown by chemical vapor deposition using a reaction of MoO<sub>3</sub> and H<sub>2</sub>S. *J. Phys. Condens. Matter* **2016**, *28*, 184002. [[CrossRef](#)] [[PubMed](#)]
10. Yu, Y.F.; Li, C.; Liu, Y.; Su, L.Q.; Zhang, Y.; Cao, L.Y. Controlled scalable synthesis of uniform, high-quality monolayer and few-layer MoS<sub>2</sub> films. *Sci. Rep.* **2013**, *3*, 1866. [[CrossRef](#)] [[PubMed](#)]
11. Lee, Y.H.; Zhang, X.Q.; Zhang, W.J.; Chang, M.T.; Lin, C.T.; Chang, K.D.; Yu, Y.C.; Wang, J.T.W.; Chang, C.S.; Li, L.J.; et al. Synthesis of large-area MoS<sub>2</sub> atomic layers with chemical vapor deposition. *Adv. Mater.* **2012**, *24*, 2320–2325. [[CrossRef](#)] [[PubMed](#)]
12. Liang, T.; Xie, S.; Huang, Z.T.; Fu, W.F.; Cai, Y.; Yang, X.; Chen, H.Z.; Ma, X.Y.; Iwai, H.; Fujita, D.; et al. Elucidation of zero-dimensional to two-dimensional growth transition in MoS<sub>2</sub> chemical vapor deposition synthesis. *Adv. Mater. Interfaces* **2017**, *4*, 1600687. [[CrossRef](#)]
13. Bampoulis, P.; van Bremen, R.; Yao, Q.R.; Poelsema, B.; Zandvliet, H.J.W.; Sotthewes, K. Defect dominated charge transport and fermi level pinning in MoS<sub>2</sub>/metal contacts. *ACS Appl. Mater. Interfaces* **2017**, *9*, 19278–19286. [[CrossRef](#)] [[PubMed](#)]
14. McDonnell, S.; Addou, R.; Buie, C.; Wallace, R.M.; Hinkle, C.L. Defect-dominated doping and contact resistance in MoS<sub>2</sub>. *ACS Nano* **2014**, *8*, 2880–2888. [[CrossRef](#)] [[PubMed](#)]
15. Zhou, W.; Zou, X.L.; Najmaei, S.; Liu, Z.; Shi, Y.M.; Kong, J.; Lou, J.; Ajayan, P.M.; Yakobson, B.I.; Idrobo, J.C. Intrinsic structural defects in monolayer molybdenum disulfide. *Nano Lett.* **2013**, *13*, 2615–2622. [[CrossRef](#)] [[PubMed](#)]
16. Addou, R.; Colombo, L.; Wallace, R.M. Surface defects on natural MoS<sub>2</sub>. *ACS Appl. Mater. Interfaces* **2015**, *7*, 11921–11929. [[CrossRef](#)] [[PubMed](#)]
17. Wang, S.S.; Rong, Y.M.; Fan, Y.; Pacios, M.; Bhaskaran, H.; He, K.; Warner, J.H. Shape evolution of monolayer MoS<sub>2</sub> crystals grown by chemical vapor deposition. *Chem. Mater.* **2014**, *26*, 6371–6379. [[CrossRef](#)]
18. Yang, S.Y.; Shim, G.W.; Seo, S.B.; Choi, S.Y. Effective shape-controlled growth of monolayer MoS<sub>2</sub> flakes by powder-based chemical vapor deposition. *Nano Res.* **2017**, *10*, 255–262. [[CrossRef](#)]
19. Wu, S.F.; Huang, C.M.; Aivazian, G.; Ross, J.S.; Cobden, D.H.; Xu, X.D. Vapor-solid growth of high optical quality MoS<sub>2</sub> monolayers with near-unity valley polarization. *ACS Nano* **2013**, *7*, 2768–2772. [[CrossRef](#)] [[PubMed](#)]
20. Jin, S.Z.; Zhao, S.C.; Weng, J.X.; Lv, Y.F. Mn-promoted growth and photoluminescence of molybdenum disulphide monolayer. *Coatings* **2017**, *7*, 78. [[CrossRef](#)]

21. Pisoni, A.; Jacimovic, J.; Barisic, O.S.; Walter, A.; Nafradi, B.; Bugnon, P.; Magrez, A.; Berger, H.; Revay, Z.; Forro, L. The role of transport agents in MoS<sub>2</sub> single crystals. *J. Phys. Chem. C* **2015**, *119*, 3918–3922. [[CrossRef](#)]
22. Castellanos-Gomez, A.; Barkelid, M.; Goossens, A.M.; Calado, V.E.; van der Zant, H.S.J.; Steele, G.A. Laser-thinning of MoS<sub>2</sub>: On demand generation of a single-layer semiconductor. *Nano Lett.* **2012**, *12*, 3187–3192. [[CrossRef](#)] [[PubMed](#)]
23. Mak, K.F.; Lee, C.; Hone, J.; Shan, J.; Heinz, T.F. Atomically thin MoS<sub>2</sub>: A new direct-gap semiconductor. *Phys. Rev. Lett.* **2010**, *105*, 136805. [[CrossRef](#)] [[PubMed](#)]
24. Splendiani, A.; Sun, L.; Zhang, Y.B.; Li, T.S.; Kim, J.; Chim, C.Y.; Galli, G.; Wang, F. Emerging photoluminescence in monolayer MoS<sub>2</sub>. *Nano Lett.* **2010**, *10*, 1271–1275. [[CrossRef](#)] [[PubMed](#)]
25. Bampoulis, P.; Teernstra, V.J.; Lohse, D.; Zandvliet, H.J.W.; Poelsema, B. Hydrophobic ice confined between graphene and MoS<sub>2</sub>. *J. Phys. Chem. C* **2016**, *120*, 27079–27084. [[CrossRef](#)]
26. Varghese, J.O.; Agbo, P.; Sutherland, A.M.; Brar, V.W.; Rossman, G.R.; Gray, H.B.; Heath, J.R. The influence of water on the optical properties of single-layer molybdenum disulfide. *Adv. Mater.* **2015**, *27*, 2734–2740. [[CrossRef](#)] [[PubMed](#)]
27. Kwiecinski, W.; Sotthewes, K.; Poelsema, B.; Zandvliet, H.J.W.; Bampoulis, P. Chemical vapor deposition growth of bilayer graphene in between molybdenum disulfide sheets. *J. Colloid Interface Sci.* **2017**, *505*, 776–782. [[CrossRef](#)] [[PubMed](#)]
28. Sim, H.; Lee, J.; Park, B.; Kim, S.J.; Kang, S.; Ryu, W.; Jun, S.C. High-concentration dispersions of exfoliated MoS<sub>2</sub> sheets stabilized by freeze-dried silk fibroin powder. *Nano Res.* **2016**, *9*, 1709–1722. [[CrossRef](#)]
29. Frindt, R.F. Single crystals of MoS<sub>2</sub> several molecular layers thick. *J. Appl. Phys.* **1966**, *37*, 1928–1929. [[CrossRef](#)]
30. Li, H.; Zhang, Q.; Yap, C.C.R.; Tay, B.K.; Edwin, T.H.T.; Olivier, A.; Baillargeat, D. From bulk to monolayer MoS<sub>2</sub>: Evolution of Raman scattering. *Adv. Funct. Mater.* **2012**, *22*, 1385–1390. [[CrossRef](#)]
31. Zhao, S.C.; Surwade, S.P.; Li, Z.T.; Liu, H.T. Photochemical oxidation of CVD-grown single layer graphene. *Nanotechnology* **2012**, *23*, 355703. [[CrossRef](#)] [[PubMed](#)]
32. Blanco, E.; Sohn, H.Y.; Han, G.; Hakobyan, K.Y. The kinetics of oxidation of molybdenite concentrate by water vapor. *Metall. Mater. Trans. B-Process Metall. Mater. Process. Sci.* **2007**, *38*, 689–693. [[CrossRef](#)]



© 2018 by the authors. Licensee MDPI, Basel, Switzerland. This article is an open access article distributed under the terms and conditions of the Creative Commons Attribution (CC BY) license (<http://creativecommons.org/licenses/by/4.0/>).